This SI replaces the original version published on 04 November 2024

Supplementary Information

Rational design of versatile 1D Ti-O-based core-shell nanostructures for efficient pollutant removal and solar fuel production

Qiang Wang[*a], Xiaoqiang Zhan[c], Chenming Fan[a,d], Xiaofan Yang[d], Bing Li[d], Hong Liu[*a], Yangjiang Wu[a], Kaihuan Zhang[a], Pengyi Tang[a,b*]

[a] 2020 X-Lab, Shanghai Institute of Microsystem and Information Technology, Chinese Academy of Sciences, 865 Changning Road, Shanghai 200050, China

[b] National Key Laboratory of Materials for Integrated Circuits, Shanghai Institute of Microsystem and Information Technology, Chinese Academy of Sciences, 865 Changning Road, Shanghai 200050, China

[c] Institute of Micro/Nano Materials and Devices, Ningbo University of Technology, 201 Fenghua Road, Ningbo 315211, China

[d] School of Mechanical and Power Engineering, East China University of Science and Technology, 130 Meilong Road, Shanghai 200237, China

Corresponding authors:

wangqiang@mail.sim.ac.cn (Q. Wang)

liuhong01@mail.sim.ac.cn (H. Liu)

py.tang@mail.sim.ac.cn (P. Tang)

This SI replaces the original version published on 04 November 2024

1. Experimental section

1.1 Materials preparation

Synthesis of $K_2Ti_6O_{13}$ nanobelts (KTO NBs). The KTO NBs were synthesized by a typical molten salt method at 1173 K, as reported in our previous work [1]. The flux-grown KTO nanobelt sample was named as KTO.

Synthesis of 1D KTO/TiO_2 core-shell NBs. The 1D KTO/TiO_2 core-shell NBs was prepared by a controlled hydrothermal phase-transformation method using the KTO NBs as precursors, as reported in our previous studies [2-3]. Note that the hydrothermal reactions were performed in *ca.* 4.5 M HNO_3 solution at 393 K holding for different time. The obtained catalyst samples were named as TKTO-1, TKTO-2 and TKTO-3, respectively, according to the reaction time (90 min, 150 min and 210 min). To obtain pure TiO_2 products, the acid hydrothermal synthesis was performed at 413 K for 900 min.

Fabrication of a floating photocatalyst sheet. The floating photocatalyst sheet was fabricated *via* drop-coating method on a carbon paper (CP, TGPH060FH, Toray Industries, Inc). Firstly, the CP was cut into 2.5*2.5 cm^2 sheets and cleaned in ethanol-water mixture. Next, a certain amount of catalyst sample was dispersed in 1 mL isopropanol under ultrasonication for 5 min. The catalyst slurry was then deposited on the CP by multiple-step drop coating, and the amount of catalyst on hydrophilic and hydrophobic sides was about 8 mg and 6 mg, respectively. To enhance the film adherence to CP substrate, a diluted Nafion solution (10 μL) in isopropanol (500 μL) was cast onto the catalyst film. Finally, the photocatalyst sheet was dried at 343 K for 12 h.

Fabrication of film photoelectrodes. The photocatalyst samples were deposited on the FTO glass substrates by a facile electrophoretic deposition method. Typically, a photocatalyst suspension was firstly prepared *via* dispersing iodine (10 mg) and catalyst powder (30 mg) in 40 mL of acetone under stirring and ultrasonication for 10 min. Then, two pre-cleaned FTO electrodes (7 Ω, 1*2 cm^2) were parallelly inserted into

the suspension and a voltage of 10 V was applied for 5 min. After deposition, the film electrodes were carefully rinsed by acetone and dried in air. To improve the connections between catalyst particles within the films, 50 μL of titanium(IV) butoxide 2-methoxyethanol solution (8 mM) as a necking agent was spin-coated on the catalyst films, and finally the integrated photoelectrodes were annealed at 623 K for 1 h.

1.2 Materials Characterizations

X-ray diffraction (XRD) patterns were obtained by a Bruker D8 ADVANCE instrument equipped with a Cu Ka radiation source. Scanning electron microscopy (SEM) measurements were performed using a field emission scanning electron microscope (Zeiss Sigma 300). Transmission electron micrographs (TEM) and energy dispersive X-ray spectrometry (EDS) analyses were recorded on a JEOL JEM-2100F microscope equipped with an OXFORD X-Max^N 100TLE spectrometer, and the corresponding high-resolution transmission electron microscopy (HRTEM) and selected-area electron diffraction (SAED) were also recorded using an accelerating voltage of 200 kV. UV-Vis diffuse reflection spectra were measured using a Shimadzu UV2600i UV-vis spectrometer using $BaSO_4$ as a reference. Photoluminescence (PL) measurements were performed using a FLS1000 fluorescence spectrometer (Edinburgh instrument Ltd, England) at room temperature. The steady PL spectra were recorded with the excitation wavelength at 350 nm, while the time-resolved PL (TRPL) spectra measured with an excitation wavelength of 378 nm and emission wavelength of 468 nm. The PL spectra of terephthalic acid (TA) solutions were measured with the excitation at 315 nm. Surface photovoltage (SPV) measurements were performed using a CEL-SPS1000 SPV spectrometer system (Beijing China Education Au-light Co. Ltd.). The surface water contact angle method using a Biolin Attension Theta Flex tensiometers. The contact angle measurements were performed using a Theta Flex optical tensiometer (Biolin Scientific, Sweden) and repeated at least twice to obtain the average values.

1.3 Evaluation of photocatalytic performances

This SI replaces the original version published on 04 November 2024

Photocatalytic performances of the designed photocatalysts were evaluated by pollutant degradation, H_2 generation and CO_2 photoreduction. The photodegradation tests were performed in a homemade reactor at room temperature using a 300 W Xe lamp (PLS-SXE300, Beijing Perfectlight Technology Co., Ltd.) as the light source. The initial concentration of Rhodamine B (RhB) and methyl orange (MO) dyes was 10 mg L^{-1} and the dosage of photocatalyst was 1.0 g L^{-1}. Whereas, 10 mg L^{-1} levofloxacin (LVF) aqueous solution with a catalyst dosage of 0.5 g L^{-1} was employed for antibiotic degradation. Prior to light irradiation, the suspension was magnetically stirred in dark to achieve the absorption-desorption equilibrium. During the photodegradation process, certain amount of suspension was taken at a given time interval and centrifuged to remove the catalyst powders. The changes of concentration were recorded by a Lambda 950 spectrophotometer to evaluate the degradation efficiency. All the experiments were duplicated and repeated at least twice.

The photocatalytic H_2 production activity of the as-prepared catalysts was evaluated by an online gas analysis system (CEL-SPH2N, Beijing China Education Aulight Co., Ltd.). Typically, 20 mg of photocatalyst was dispersed into 100 ml of deionized water by ultrasonication and stirring in a quartz reactor containing Na_2SO_3 (0.35 M) and Na_2S (0.25 M) as hole sacrificial agent. The photocatalysts were loaded with 1.0 wt% Pt co-catalyst via in-situ photoreduction in the diluted H_2PtCl_6 aqueous solution. The whole closed loop system was degassed until no bubbles were generated from the suspension. A 300W Xenon lamp (CEL-HXF300, Beijing China Education Aulight Co., Ltd.) placed on the top of the quartz reactor was used as the light source. The temperature of reaction cell was kept at 279 K using circulating cooling water jacket during the photocatalytic reaction. The amount of produced H_2 gas was measured at 60 min intervals using an on-line gas chromatograph (GC-7920) equipped with a thermal conductivity detector (TCD).

The photocatalytic CO_2 reduction was performed in an airtight gas-solid reactor at 288 K, as described in our previous studies. In brief, 20 mg of catalyst was uniformly

coated on a square quartz plate (2.5 × 2.5 cm^2) and placed at the bottom of the reactor. Prior to light irradiation, the enclosed gas in reactor was removed by N_2 flow, and then high-purity CO_2 (99.99%) was bubbled through DI water to fill the reactor with gaseous CO_2 and H_2O. The CEL-HXF300 Xe lamp was used as the light source, and the light intensity at the upper position of photocatalyst plate was *ca.* 270 mw cm^{-2}. After the photocatalytic reaction for 3 hours, 1 mL of gas was extracted from the reactor and quantified by a Shimadzu GC-2014 gas chromatography equipped with a flame ionization detector (FID). Twice-repeated experiments were performed for CO_2 photoreduction.

1.4 Dye pollutant removal

Selective adsorption of cationic dye. TKTO-2 sample was collected *via* washing and filtration treatment. After dried in an oven, the block samples with different shapes were annealed at 623 K for 1 h. A typical organic dye of MB was used as a probe molecule to evaluate the adsorptive ability of TKTO-2. Dye removal efficiency was determined by measuring the absorbance of MB solutions at 646 nm before and after adsorption test using Shimadzu 2600i UV-vis spectrophotometer.

Dye removal by floating photocatalyst sheet. As for MB removal *via* adsorption and photothermal catalysis processes, the photocatalyst/CP sheet was floated on the MB solution (10 mg L^{-1}, 40 mL) with the hydrophilic side down and hydrophobic side up. Note that the glass reactor was covered by aluminum foil to reduce light loss and improve the light harvesting of photocatalysts on the hydrophilic side. During the reaction process, the temperature at the surface of photocatalyst/CP sheet was monitored. The absorbance changes of MB solutions at certain intervals were measured by Shimadzu 2600i UV-vis spectrophotometer. For comparison, the blank tests with and without the bare CP sheet were also performed.

1.5 Photoelectrocatalytic (PEC) measurements

PEC water-splitting measurements were performed in a standard three-electrode

system using 1.0 M NaOH as electrolyte (pH=13.6). The as-prepared photocatalyst films, Pt sheet and Ag/AgCl electrode were used as the working electrode, counter electrode and reference electrode, respectively. The simulated sunlight irradiation was supported by the CEL-S500 system equipped with AM1.5G filter and the light intensity was adjusted to 100 mW cm^{-2}. As for PEC glycerol oxidation, the electrolyte containing 0.1 M glycerol and 1M NaOH was used. The liquid products in the anodic section can be measured by ion chromatography (IC, Dionex ICS 3000). The in-situ differential electrochemical mass spectrometry (DEMS) measurements were performed to determine the gas products in the PEC cell using a QAS 100 device (Shanghai Linglu Instruments and Equipment Co., Ltd.).

1.6 Computational details

The DFT calculations were performed using the Vienna Ab initio Simulation Package (VASP) code [4], which employs the projector augmented wave (PAW) method [5-8]. The generalized gradient approximation (GGA) with Perdew-Burke-Ernzerhof (PBE) exchange-correlation functional was applied to define the plane wave basis [9], and the cutoff was 500 eV. The atomic configurations were allowed to relax until residual force were below the threshold of 0.05 eV/Å, and an energy convergence criterion of 1×10−4 eV. To mitigate the influence of periodic boundary conditions on the slab, the vacuum thicknesses were set more than 15 Å. Considering that $K_2Ti_6O_{13}$ have different lattice constants compared to TiO_2, heterojunction models with different supercells were constructed. Details are shown in **Table S1**.

Table S1. Supercell lattices and lattice mismatch degree of the heterojunction models.

Heterojunction model	a Å	b Å	Mismatch degree	
			a (%)	b (%)
$TiO_2/K_2Ti_6O_{13}$	9.06	27.03	1.81	0.44

This SI replaces the original version published on 04 November 2024

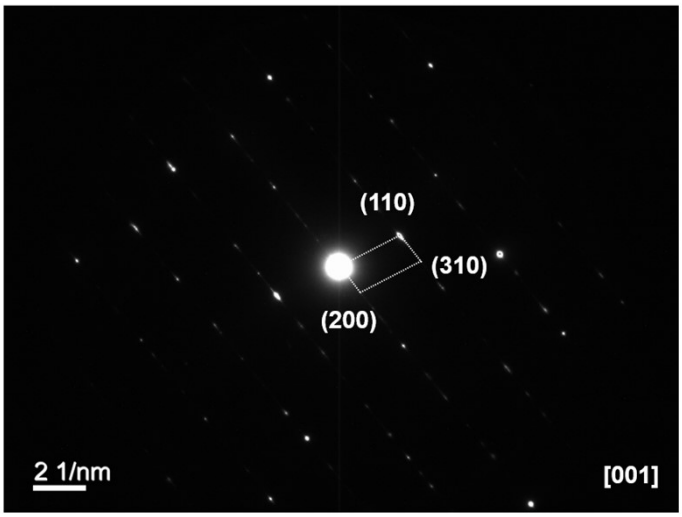

Figure S1 The SAED pattern of TKTO-2 NBs assigned to the monoclinic $K_2Ti_6O_{13}$ phase.

This SI replaces the original version published on 04 November 2024

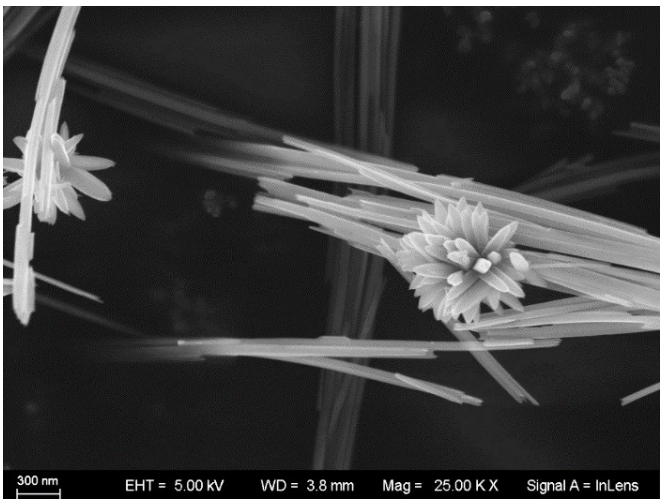

Figure S2 A typical SEM image of the as-synthesized TKTO-3 sample.

This SI replaces the original version published on 04 November 2024

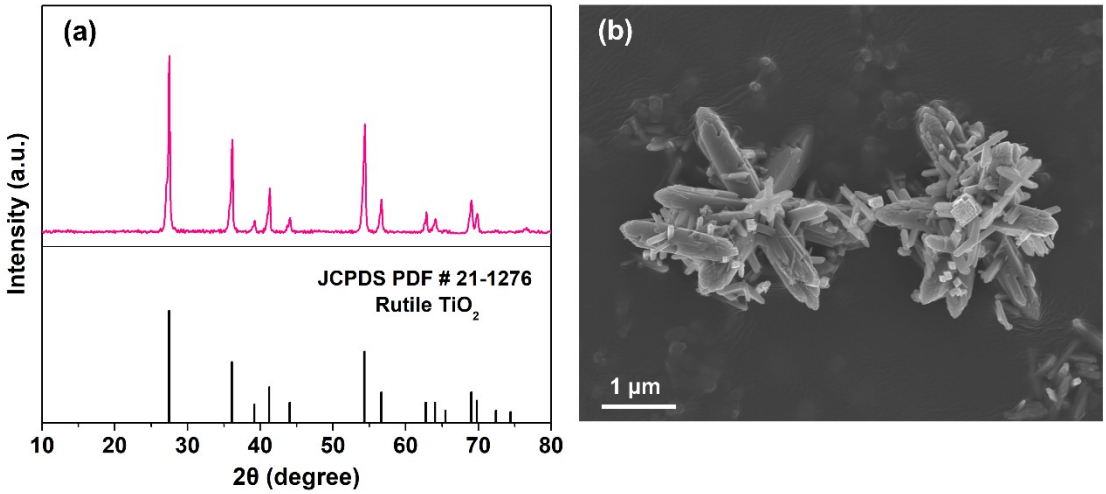

Figure S3 (a) XRD pattern and (b) a typical TEM image of the synthesized TiO_2 sample.

This SI replaces the original version published on 04 November 2024

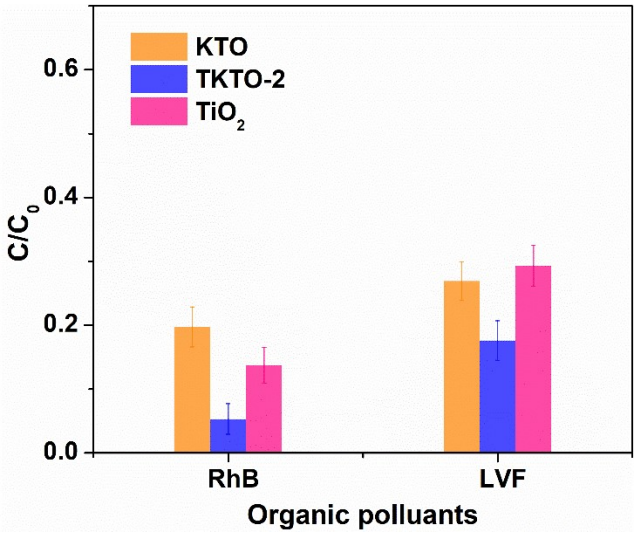

Figure S4 Photocatalytic degradation of RhB (light irradiation 120 min) and LVF (light irradiation 80 min) over the synthesized samples.

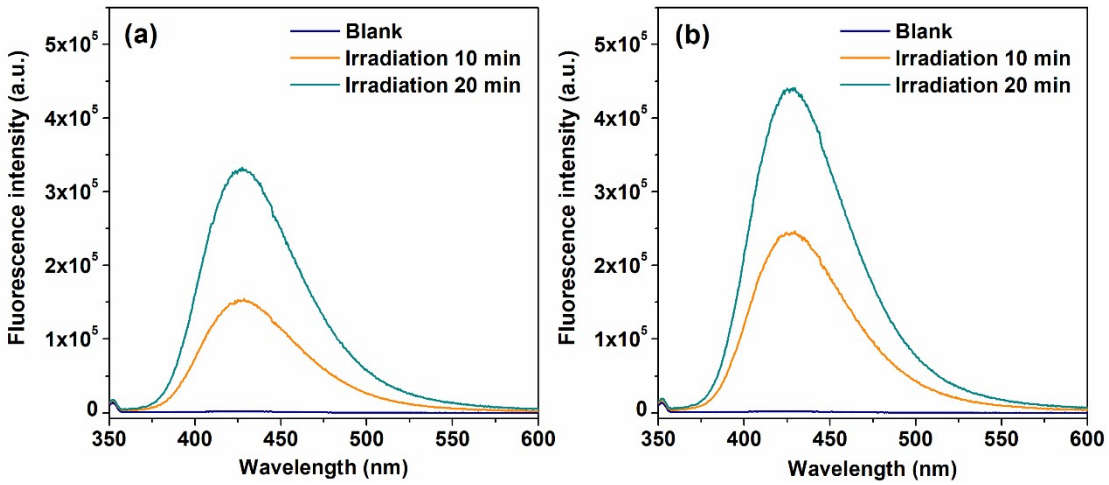

Figure S5 PL spectra of TA solutions in the presence of KTO (a) and TKTO-2 (b) photocatalysts under light irradiation.

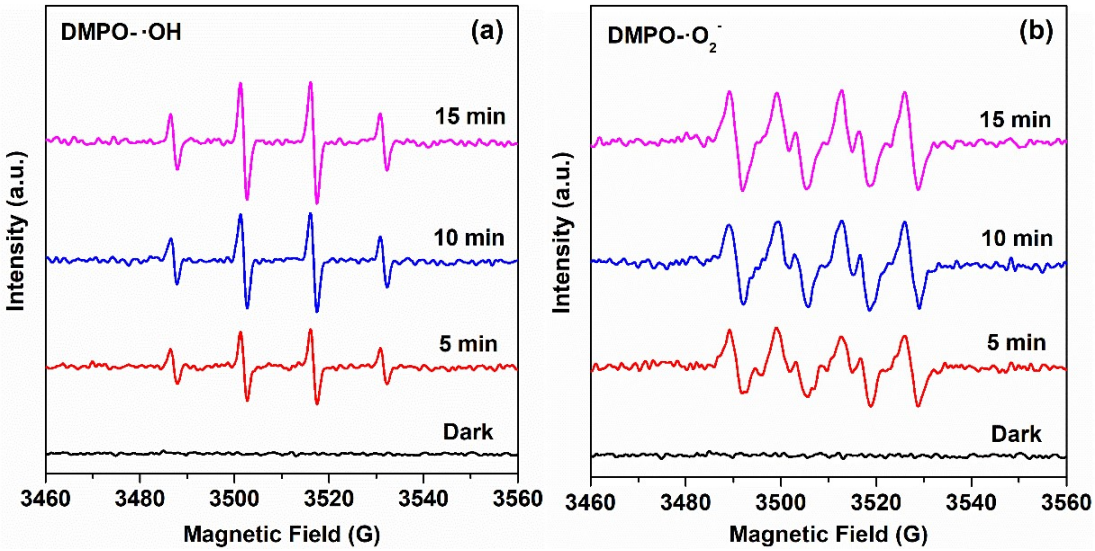

Figure S6 ESR spectra of (a) DMPO-·OH and (b) DMPO-·O_2^- in the presence of TKTO-2 photocatalyst under light irradiation.

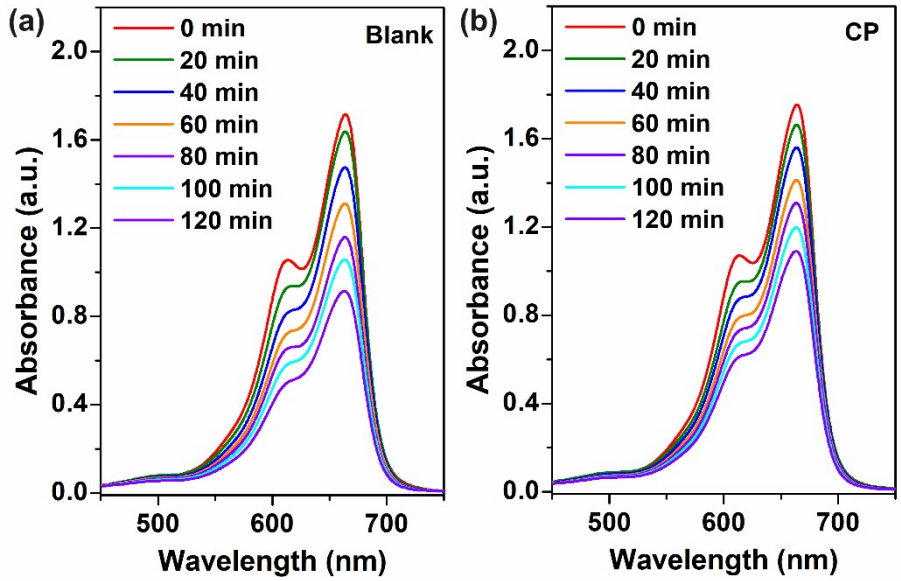

Figure S7 UV-vis spectra of MB solutions in the absence of any photocatalysts (a) and over CP sheet (b) with different irradiation time.

This SI replaces the original version published on 04 November 2024

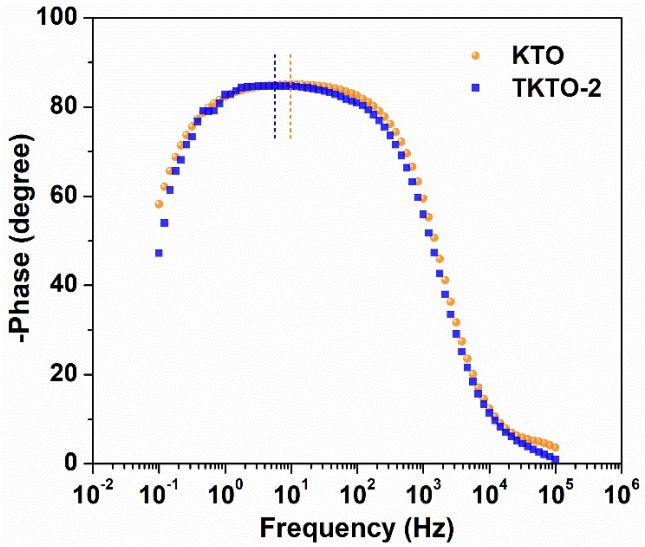

Fig. S8 Bode plots of KTO and TKTO-2 electrodes.

This SI replaces the original version published on 04 November 2024

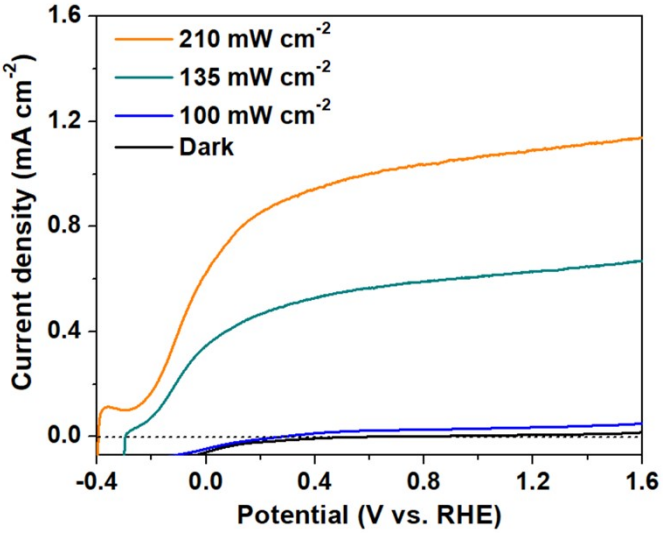

Figure S9 LSV curves of KTO photoanode for GOR under the different light irradiation.

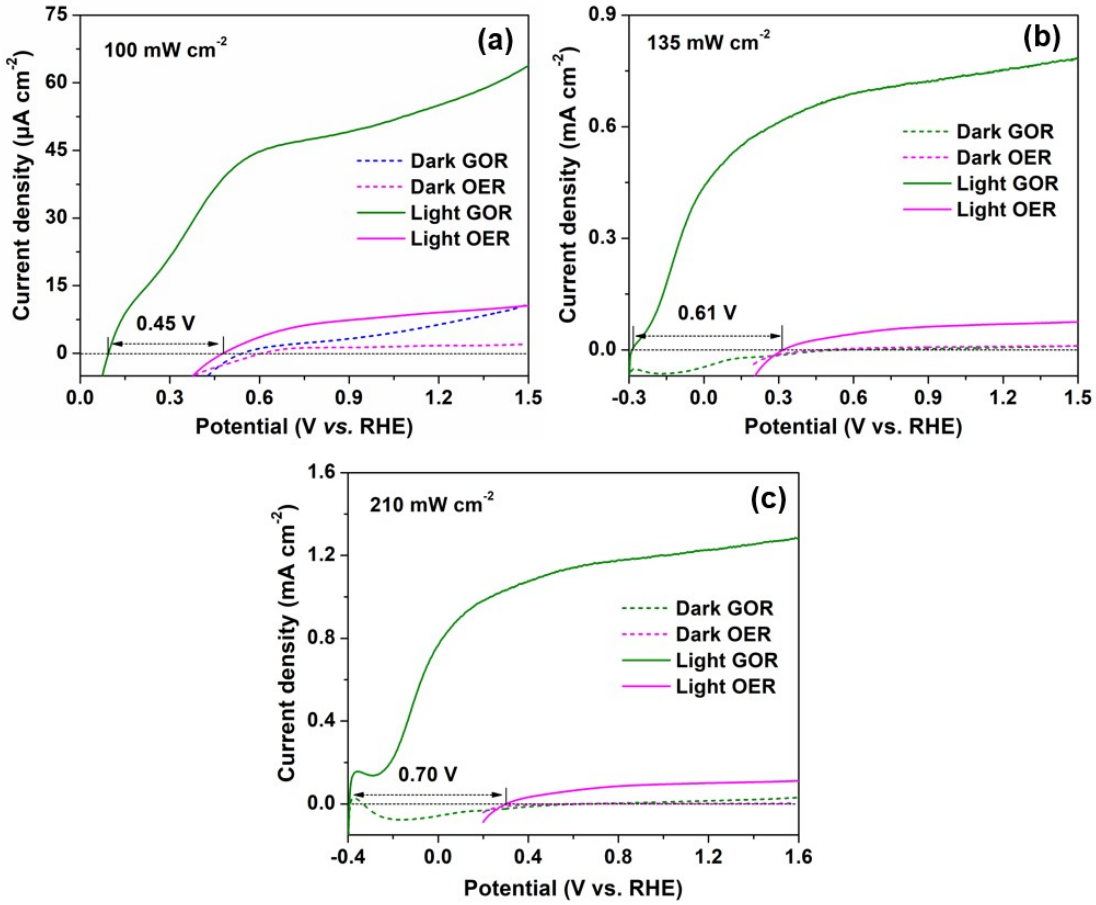

Figure S10 LSV curves of TKTO-2 photoanode for OER and GOR under the different light irradiation: (a) 100 mW cm^{-2}, (b) 135 mW cm^{-2}, (c) 210 mW cm^{-2}.

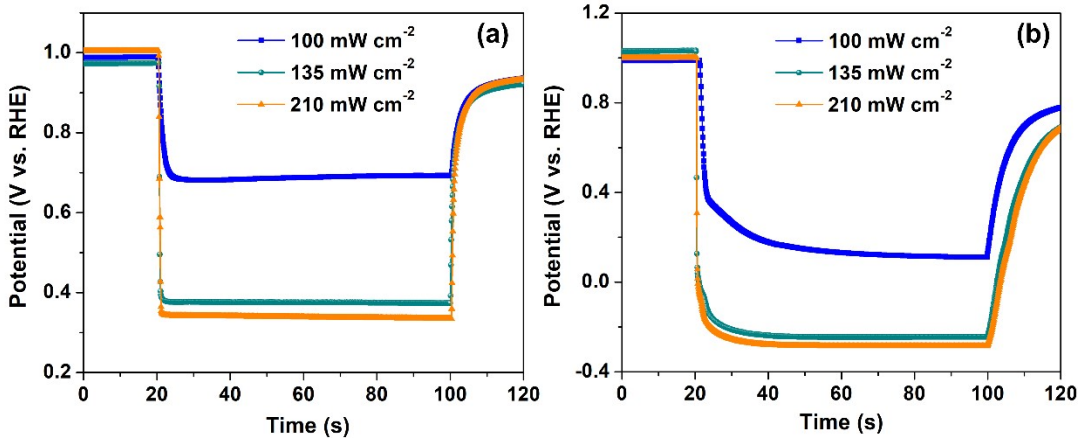

Figure S11 V_{oc} responses of TKTO-2 photoanode in the different reaction systems: (a) 1 M NaOH solution, (b) 1M NaOH/0.1 M glycerol mixture.

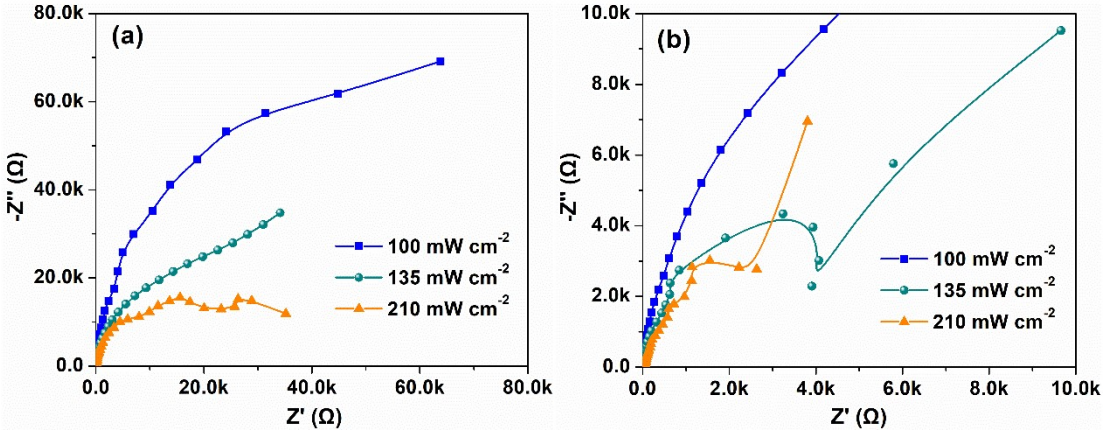

Figure S12 EIS analysis of the TKTO-2 photoanode at 1.23 V vs. RHE in different reaction systems: (a) 1 M NaOH solution, (b) 1M NaOH/0.1 M glycerol mixture.

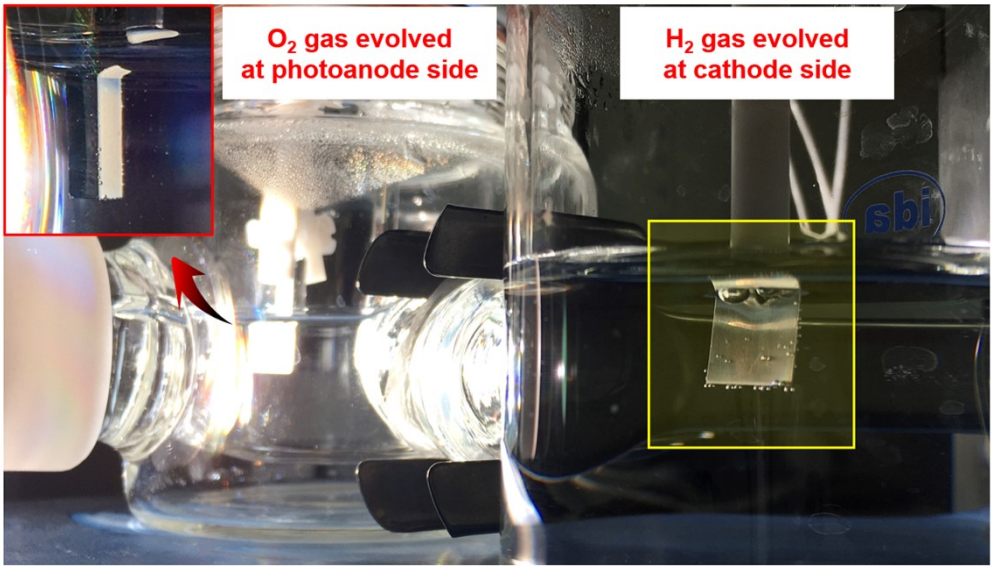

Figure S13 Photos of the H-type PEC cell in NaOH/glycerol electrolyte operated at 1.23 V_{RHE} under 135 mW cm^{-2} irradiation, showing the O_2 gas bubbles evolved at photoanode side and H_2 gas bubbles evolved at Pt cathode side.

This SI replaces the original version published on 04 November 2024

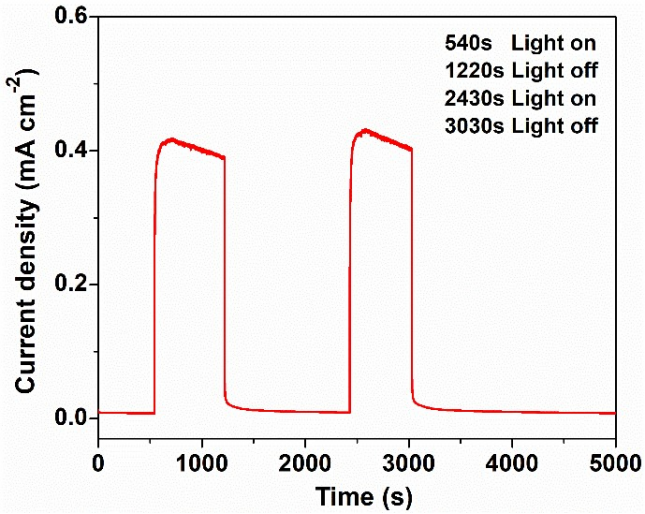

Figure S14 Photocurrent density of TKTO-2 photoanode at 1.23 V_{RHE} for the in-situ DEMS test.

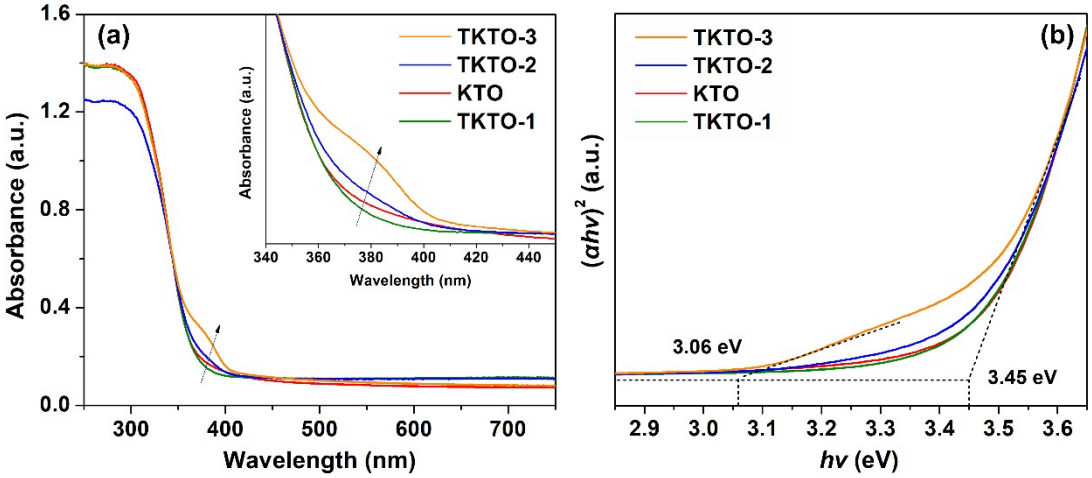

Figure S15 (a) UV-vis spectra and the corresponding Tauc plots of the as-synthesized samples.

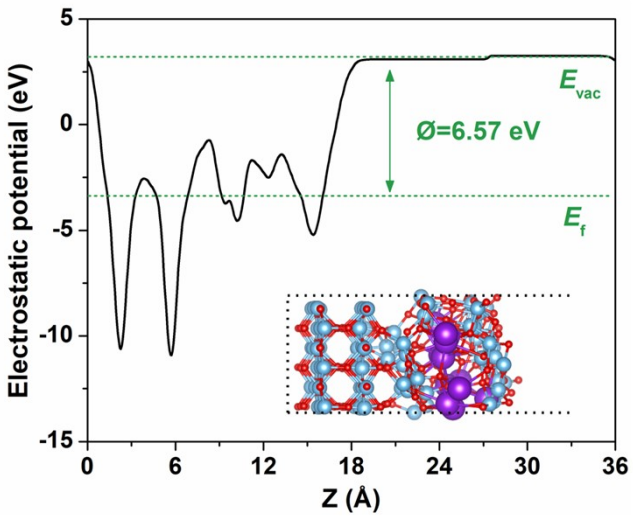

Figure S16 The calculated electrostatic potential of KTO/TiO_2 heterojunction.

This SI replaces the original version published on 04 November 2024

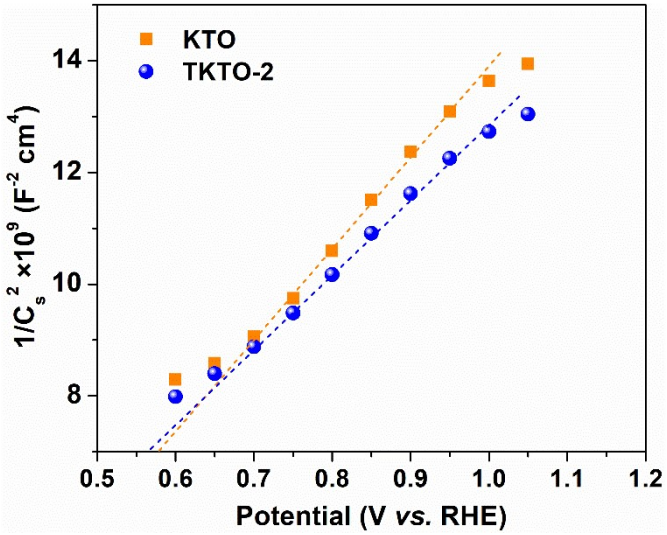

Figure S17 Mott-Schottky plots of KTO and TKTO-2 samples at 1000 Hz in 1.0 M NaOH under AM 1.5G irradiation.

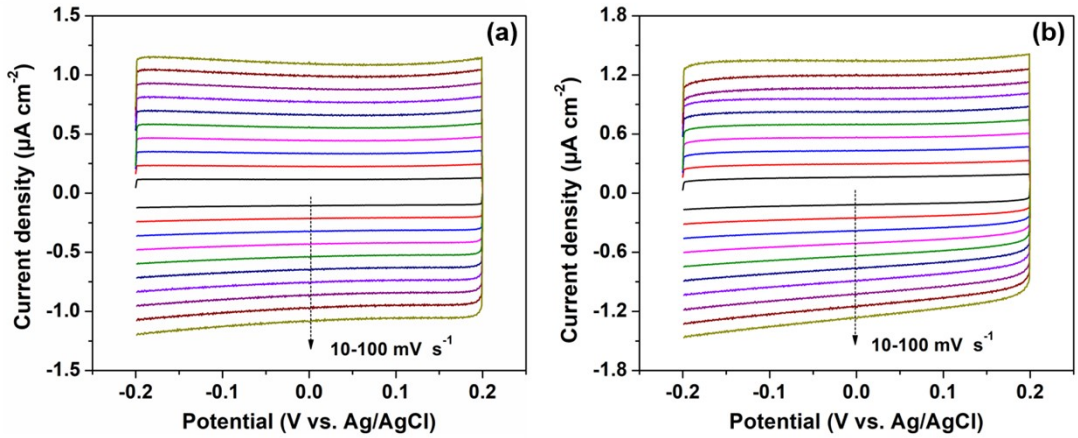

Figure S18 Cyclic voltammetry curves of KTO (a) and TKTO-2 in 1.0 M NaOH without light irradiation.

This SI replaces the original version published on 04 November 2024

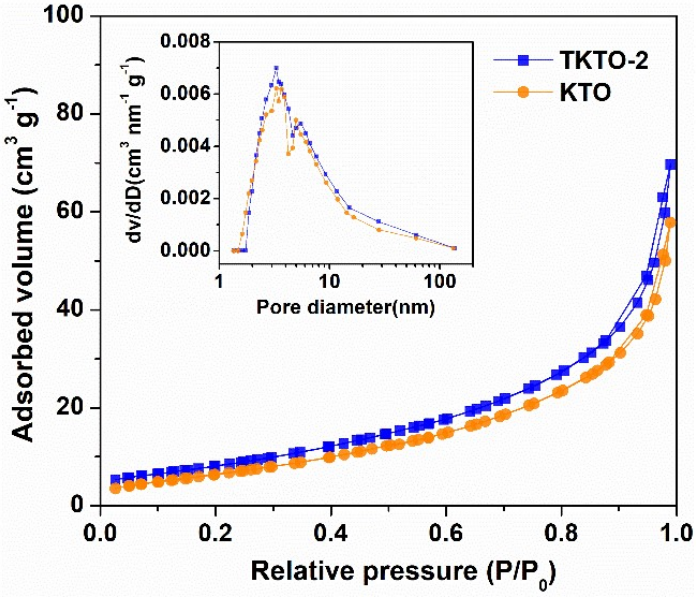

Figure S19 N_2 adsorption-desorption isotherms and BJH pore size distribution curves (inset) of KTO and TKTO-2.

This SI replaces the original version published on 04 November 2024

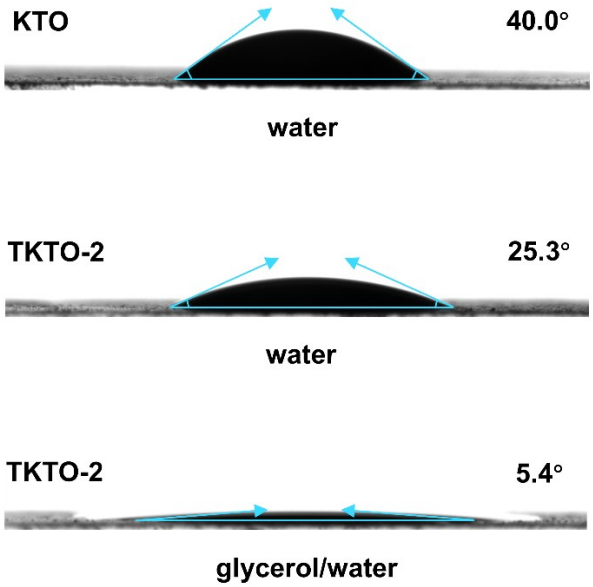

Figure S20 The contact angles of KTO and TKTO-2 photoanodes.

This SI replaces the original version published on 04 November 2024

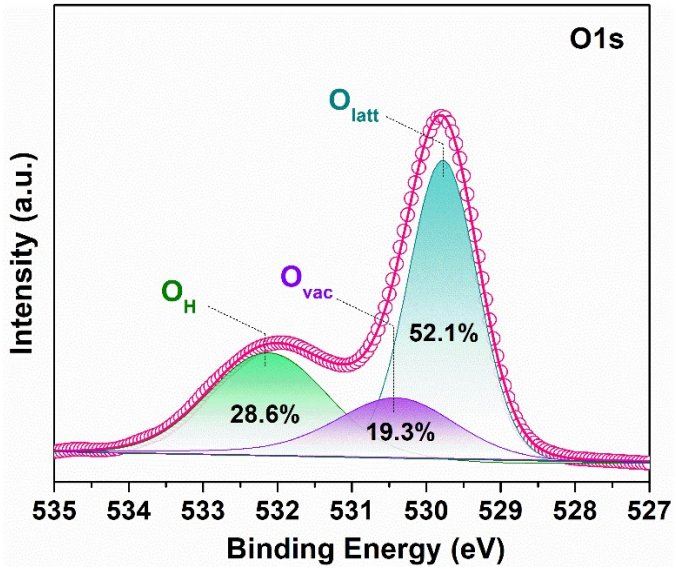

Figure S21 High-resolution O1s XPS spectrum of the synthesized pure TiO_2 sample.

This SI replaces the original version published on 04 November 2024

Table S2 The percentage of various oxygen peaks in the fitted O1s XPS spectra of the synthesized samples.

Sample	Percentage of the fitted oxygen peaks (%)		
	O_{latt}	O_{vac}	O_H
KTO	78.4	15.6	6.0
TKTO-2	74.1	17.1	8.8
TiO_2	52.1	19.3	28.6

This SI replaces the original version published on 04 November 2024

References

[1] Q. Wang, B. Zhang, X. Lu, X. Zhang, H. Zhu, B. Li, Multifunctional 3D $K_2Ti_6O_{13}$ nanobelt-built architectures towards wastewater remediation: selective adsorption, photodegradation, mechanism insight and photoelectrochemical investigation, Catal. Sci. Technol., 8 (2018) 6180-6195.

[2] Q. Wang, H. Zhu, B. Li, Synergy of Ti-O-based heterojunction and hierarchical 1D nanobelt/3D microflower heteroarchitectures for enhanced photocatalytic tetracycline degradation and photoelectrochemical water splitting, Chem. Eng. J., 378 (2019) 122072.

[3] Q. Wang, C. Fan, G. Li, J. Luo, B. Li, Unique 1D/3D $K_2Ti_6O_{13}/TiO_2$ micro-nano heteroarchitectures: controlled hydrothermal crystal growth and enhanced photocatalytic performance for water purification, Catal. Sci. Technol., 9 (2019) 7023-7033.

[4] J. Hafner, Ab-initio simulations of materials using VASP: Density-functional theory and beyond, J. Comput. Chem., 29 (2008) 2044.

[5] P.E. Blöchl, Projector augmented-wave method, Phys. Rev. B, 50 (1994) 17953-17979.

[6] G. Kresse, J. Furthmüller, Efficient iterative schemes for ab initio total-energy calculations using a plane-wave basis set., Phys. Rev. B, 54 (1996) 11169-11186.

[7] G. Kresse, J. Furthmüller, Efficiency of ab-initio total energy calculations for metals and semiconductors using a plane-wave basis set, Comput. Mater. Sci., 6 (1996) 15-50.

[8] G. Kresse, D. Joubert, From ultrasoft pseudopotentials to the projector augmented-wave method, Phys. Rev. B, 59 (1999) 1758-1775.

[9] J.P. Perdew, K. Burke, M. Ernzerhof, Generalized gradient approximation made simple, Phys. Rev. Lett., 77 (1996) 3865-3868.